ISSN 0023-1584, Kinetics and Catalysis, 2010, Vol. 51, No. 2, pp. 154–161. © Pleiades Publishing, Ltd., 2010.
Original Russian Text © O.P. Korobeinichev, I.V. Rybitskaya, A.G. Shmakov, A.A. Chernov, T.A. Bolshova, V.M. Shvartsberg, 2010, published in Kinetika i Kataliz, 2010, Vol. 51, No. 2, pp. 168–175.

Mechanism of Inhibition of Hydrogen/Oxygen Flames of Various Compositions by Trimethyl Phosphate

O. P. Korobeinichev, I. V. Rybitskaya, A. G. Shmakov, A. A. Chernov, T. A. Bolshova, and V. M. Shvartsberg

Institute of Chemical Kinetics and Combustion, Siberian Branch, Russian Academy of Sciences, Novosibirsk, 630090 Russia
e-mail: korobein@kinetics.nsc.ru

Received December 5, 2008

Abstract—The effect of the catalytic recombination reactions of H and $OH^{\bullet}$ involving phosphorus-containing products of trimethyl phosphate (TMP) combustion on the burning velocity and the structure of $H_2/O_2/N_2$ flames at atmospheric pressure has been investigated. An earlier mechanism for inhibition of rich hydrogen/oxygen flames by organophosphorus compounds has been tested and modified by comparing experimental data with the results of simulation. The sensitivity analysis of the calculated flame speed to the rate constants of chain branching reactions and chain termination reactions involving phosphorus-containing compounds has revealed significant specific features of the inhibition mechanism of hydrogen flames with various stoichiometries and dilution ratios. Unlike the inhibition efficiency of hydrocarbon flames, in which the reactions of H and $OH^{\bullet}$ radicals with PO, PO_2, HOPO, and $HOPO_2$ play the key role, the inhibition efficiency of hydrogen flames at atmospheric pressure is determined by the interaction of hydrogen and oxygen atoms with TMP and with organophosphorus products of its decomposition in the low-temperature zone of the flame. The sensitivity analysis has demonstrated that, as the equivalence ratio (ϕ) or the dilution ratio is increased, the ratio of the chain branching rate to the rate of chain termination via reactions involving phosphorus compounds decreases. As a consequence, the efficiency of inhibition of $H_2/O_2/N_2$ flames, as distinct from that of hydrocarbon flames, increases as ϕ is raised from 1.1 to 3.0 and as the mixture is progressively diluted with nitrogen.

DOI: 10.1134/S0023158410020023

The data available on the kinetic mechanisms for inhibition were derived from measurements of macro characteristics of combustion (limits, ignition delays, etc.). This is explained by lack of experimental data on the chain carrier concentration in the flame, particularly at atmospheric pressure. Convenient objects for study are organophosphorus compounds (OPCs), which are mainly used for the inhibition of hydrocarbon flames.

In recent decades, a number of researchers have demonstrated that OPC combustion products can catalyze the recombination of chain carriers in the flame and are, therefore, effective hydrocarbon flame inhibitors and flame suppressants [1–7]. However, OPCs (up to 0.5 vol %) introduced into a hydrogen flame at a low pressure (50 Torr) produce a promoting effect, raising the flame speed and temperature [8]. The mechanisms for hydrocarbon flame inhibition and hydrogen flame promotion by OPC additives are based on the same atom and free radical recombination processes catalyzed by phosphorus oxides and phosphoric acids—OPCs combustion products.

Several mechanisms for flame inhibition and promotion by OPCs have been developed. The latest, best substantiated and most complete version was developed from experimental burning velocity data for premixed trimethyl phosphate–doped C_3H_8/air flames using methods of quantum chemistry [9, 10]. This version was used in the interpretation of a large amount of experimental data, including quenching conditions [11] and the structures of diffusion [12] and premixed [13] hydrocarbon/air flames doped with OPCs.

The inhibition mechanism is based on reactions forming a number of interlinked catalytic cycles of the recombination of active flame species [10]. Each cycle plays its own role, which depends on the composition of the phosphorus-containing products of OPC combustion, on the flame temperature, and on the stoichiometry of the unburned gases.

This mechanism satisfactorily predicts the flame structure and burning velocity for lean and stoichiometric CH_4/air and C_3H_8/air mixtures, but it provides a much worse fit to the concentration profiles of labile species in rich flames [13]. The following assumption was made to explain the much lower inhibition effi-

ciency for flames with $\phi > 1.2$–1.3 [13] and the discrepancy between calculated and experimental data. Under conditions of a considerable fuel excess, trimethyl phosphate (TMP) combustion is incomplete, resulting in low-active carbon- and phosphorus-containing species not considered by the model. It is, therefore, of interest to verify the above assumption and to refine the mechanism of the reactions involving OPCs in a simpler, hydrogen/oxygen flame containing no carbon. The purpose of this work was to study the effect of OPC admixtures on the burning velocity and structure of atmospheric-pressure $H_2/O_2/N_2$ flames of various compositions and to validate the earlier developed inhibition mechanism by comparing experimental data and modeling data.

EXPERIMENTAL

Flame Speed Measurement

The normal flame speed was measured by the heat flux method [14, 15]. The experimental setup was the same as described in [16]. The experimental techniques used in this works are reported elsewhere [13].

Flame Structure Measurement

Premixed $H_2/O_2/N_2$ flames were stabilized at 1 atm on a flat burner described in our earlier work [13]. The concentration profiles of flame components were measured by molecular-beam mass spectrometry (MS7302 quadrupole mass spectrometer) with soft electron-impact ionization [17]. The combustion products were sampled from the flame using a quartz cone with a orifice diameter of 0.08 mm and an inner angle of 40°. The intensities of mass peaks due to H, $OH^{\bullet}$, and phosphorus-containing species were measured at lowered ionizing electron energies. This allowed the contributions from fragment ions to the measured peaks to be avoided. The ionization energies for each peak are presented in [17].

The systematic error in mass peak intensities depended strongly on the concentration of the corresponding compound in the flame and on the background level and did not exceed 5 rel % for stable components; 10–15% for H and $OH^{\bullet}$; 15% for PO, PO_2, and HOPO; 20% for $HOPO_2$; and 30% for $(HO)_3PO$.

The calibration coefficients for H, O, and $OH^{\bullet}$ were derived from the partial equilibrium condition for the three fast reactions $H_2 + OH^{\bullet} = H_2O + H$, $H_2 + O = H + OH^{\bullet}$, and $O_2 + H = OH^{\bullet} + O$ as described in our earlier work [18]. The $\phi = 1.1$ flame with a dilution ratio of $D = [O_2]/([O_2] + [N_2]) = 0.140$ was chosen for calibration. The H_2, O_2, and H_2O concentrations in the post-flame zone of this flame are sufficiently high to be measured with a satisfactory of accuracy. The calibration coefficients determined in this way were used to calculate radical concentrations in other flames. According to our estimates, the standard error in the concentrations determined by this method is ±50%.

Temperature Measurements

Temperature profiles in flames were measured with a Π-shaped Pt/(Pt + 10% Rh) thermocouple welded from 0.02-mm wires and protected with a thin SiO_2 layer to prevent the catalytic recombination of radicals on the thermocouple surface. The thermojunction was placed at a distance of 0.25 mm from the probe orifice. A more detailed description of the temperature measurements is presented elsewhere [19].

SIMULATION

In flame structure and burning velocity simulations, we used the PREMIX and CHEMKIN programs. The flame structure was calculated using experimentally measured temperature profile. A kinetic mechanism consisting of 210 steps and involving 41 compounds [10] was also used in the simulation.

RESULTS AND DISCUSSION

Effect of the Equivalence Ratio and Nitrogen Dilution Ratio on the Speed of the TMP-Doped $H_2/O_2/N_2$ Flame

Figure 1 plots the observed $H_2/O_2/N_2$ flame speed versus ϕ in the 0.3–2.8 range for various D values between 0.077 and 0.209. Figure 1 also presents the data obtained using the counterflow burner technique [20] for a combustible mixture at room temperature and converted to our experimental conditions (T_0 = 35°C). The good agreement between our data and the literature is evidence that our measurements are correct. The flame speeds predicted by the model are somewhat lower than the corresponding experimental data.

The introduction of 0.4 vol % TMP into the flame causes a marked decrease in the burning velocity. The flame speed as a function of the equivalence ratio was also measured and calculated for flames doped with 0.04% TMP. The experimental and calculated data in this case differ by a factor of 1.3–2. However, this discrepancy is not due to systematic errors in these measurements. The discrepancy between the observed and predicted burning velocities for the TMP-doped flame and the same discrepancy for the TMP-free flame are opposite in sign: the model leads to an overestimated

Key reactions responsible for inhibition, the preexponential factors of their rate constants according to [10], and those used in this study

Reaction	A [10]*	A*
$(CH_3O)_3PO + H = (CH_3O)_2PO(OCH_2) + H_2$	2.2×10^9	4.4×10^9
$(CH_3O)_2PO(OCH_2) + O = OP(OCH_3)_2O + CH_2O$	5.0×10^{13}	1.0×10^{13}
$(CH_3O)_2PO(OCH_2) = OP(OCH_3)_2 + CH_2O$	2.0×10^{13}	2.0×10^{12}

* The preexponential factors are expressed in units of $cm^3\ mol^{-1}\ s^{-1}$ for the second-order reactions and s^{-1} for the first-order reaction.

propagation rate for the undoped flame and to an underestimated value for the doped flame.

The sensitivity analysis of the burning velocity of the TMP-doped $H_2/O_2/N_2$ flame to the rate constants of the reactions involving phosphorus-containing compounds demonstrated that the speed of the hydrogen flame, unlike that of hydrocarbon/air flames depends strongly on the primary stages of TMP destruction and its primary decomposition products, which take place in the pre-flame zone. The relevant reactions are presented in the table. Note that the propagation rate of methane/air and propane/air flames is most strongly affected by atom and radical recombination reactions involving phosphorus oxides and phosphoric acids, which take place in the high-temperature zone of the flame [17]. Because the rate constants of the reactions listed in the table were previously estimated only approximately [21], we changed the preexponential factors of these constants in order to reconcile the calculated and observed flame burning velocities (see the table).

The flame speeds calculated using modified values of the rate constants of three reactions and the corresponding experimental data are presented in Fig. 2. It is clear from Fig. 2 that the modified mechanism is in satisfactory agreement with the experimental data. Note that the sensitivity coefficients of these reactions for the TMP-doped CH_4/air flame are negligibly small. For example, the speeds of the CH_4/air flame ($\phi = 1.1$, 0.6% TMP) calculated for the initial mechanism and for the mechanism with modified rate constants of the three reactions differ only by 0.2%. Thus, the modified mechanism correctly predicts the burning velocity both for TMP-doped hydrocarbon flames and for TMP-doped hydrogen flames. Calculations demonstrated that changing the rate constants of these three reactions does not lead to any noticeable change

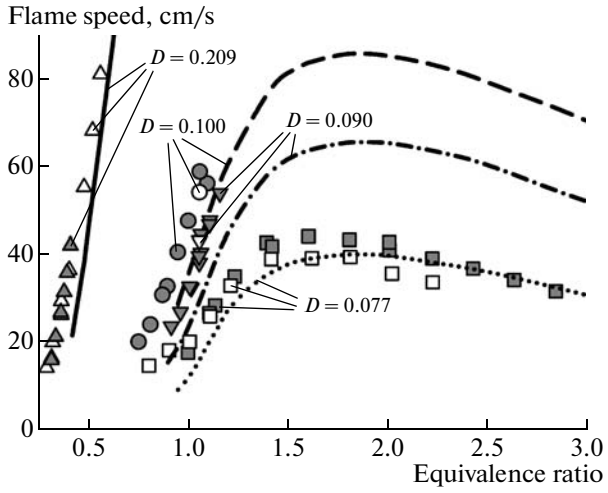

Fig. 1. Speed of $H_2/O_2/N_2$ flames with various dilution ratios (D) as a function of the equivalence ratio (ϕ). The points represent experimental data (gray symbols, data of this study; open symbols, data from [20]), and the lines represent the results of simulation.

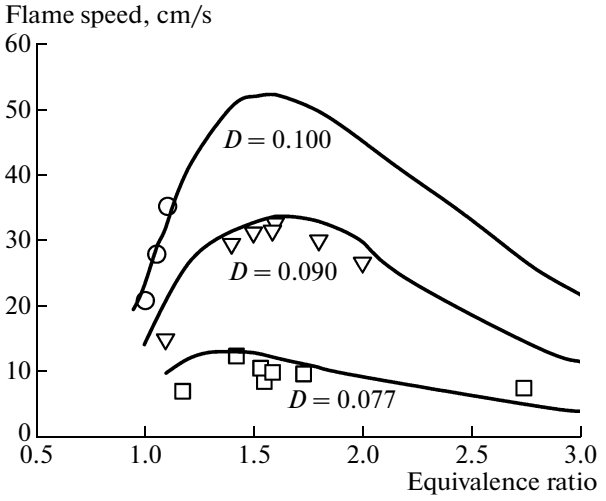

Fig. 2. Speed of $H_2/O_2/N_2$ flames with various dilution ratios (D) in the presence of 0.04 vol % TMP as a function of the equivalence ratio (ϕ). The points represent experimental data, and the lines represent the results of simulation using the modified mechanism.

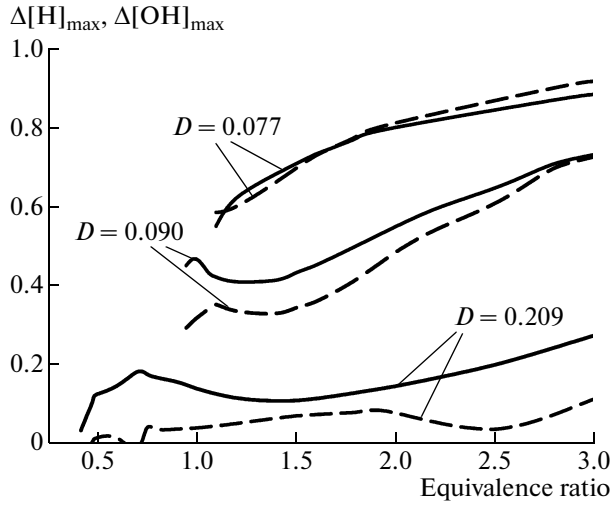

Fig. 3. Relative changes in the maximum concentrations of H (solid lines) and $OH^{\bullet}$ (dashed lines) in flames with various dilution ratios (D) in the presence of 0.04% TMP as a function of the equivalence ratio (simulation using the modified mechanism).

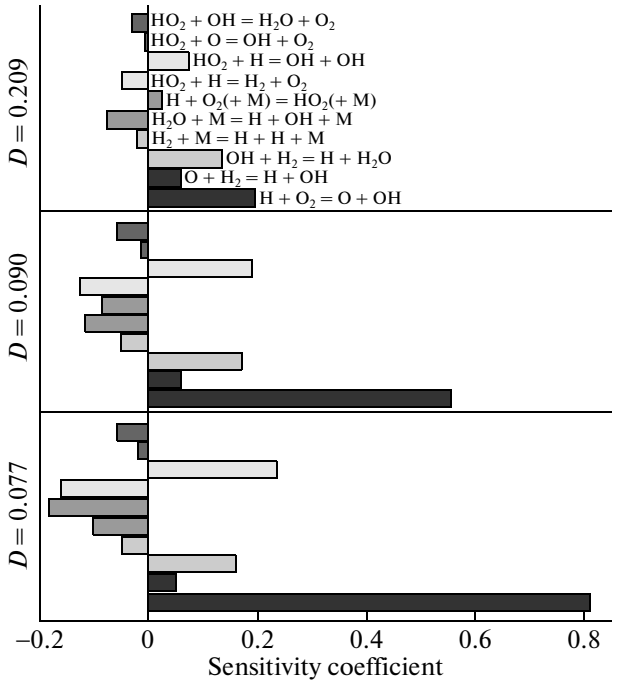

Fig. 4. Sensitivity of the speed of $H_2/O_2/N_2$ flames (ϕ = 1.6; D = 0.077, 0.090, 0.209) doped with 0.04% TMP to the rate constants of the ten most important reactions of the hydrogen oxidation mechanism.

in the structure of the $\phi = 1.6$ flame, including the concentration profiles of the final TMP conversion products—PO, PO_2, HOPO, and $HOPO_2$.

From the results of simulations using the modified mechanism, we derived the flame inhibition efficiency F as function of ϕ: $F = (U_0 - U)/U_0$, where U_0 and U are the flame propagation rates in the absence of an admixture and in the presence of 0.04 vol % TMP, respectively. It was found that the inhibition efficiency F increases as ϕ is increased from 1 to 3 and as D is decreased from 0.209 to 0.077. The results of simulation for the $D = 0.077$ flame are in good agreement with experimental data.

It is significant that the $F(\phi)$ data for hydrogen and hydrocarbon flames are fairly different [13, 22]. For hydrocarbon flames doped with 0.06 vol % TMP, F increases slightly as ϕ is raised from 0.7 to 1.2–1.3 and decreases by a factor of 1.5–2 as ϕ is further increased from 1.3 to 1.5 [13].

The introduction of TMP into the flame reduces the maximum concentration of H atoms in the chemical reaction zone. Figure 3 plots the TMP-induced relative decrease in the concentrations of H atoms ($\Delta[H]_{max} = 1 - [H]^d_{max}/[H]^0_{max}$) and $OH^{\bullet}$ radicals ($\Delta[OH]_{max} = 1 - [OH]^d_{max}/[OH]^0_{max}$) as a function of ϕ. These curves were derived from the calculated structures of freely propagating undoped and TMP-doped (0.04%) flames. Here, $[H]_{max}$ and $[OH]_{max}$ are the maximum H and $OH^{\bullet}$ concentrations in the flame zone and the subscripts d and 0 designate the TM-doped and undoped flames, respectively. It is clear from the dependence of F on ϕ [22] and the curves in Fig. 3 that there is a correlation between all these dependences (F, $\Delta[H]_{max}$ and $\Delta[OH]_{max}$).

The sensitivity analysis of the flame speed at D = 0.090 to reaction rate constants demonstrated that the role of the reactions given below increases considerably as ϕ rises from 1.1 to 1.9,

$$(CH_3O)_3PO + H = (CH_2O)(CH_3O)_2PO + H_2, \quad (I)$$

$$(CH_2O)(CH_3O)_2PO + H = (CH_3O)_3PO, \quad (II)$$

$$HOPO + H = H_2 + PO_2. \quad (III)$$

These reactions are part of the catalytic cycles of the recombination of H atoms into H_2. It is due to these reactions that the inhibition efficiency grows with increasing ϕ. Discussing the catalytic cycles of radical recombination in OPC-doped flames, we usually mean reactions involving phosphorus oxides and phosphoric acids since the reactions of OPCs generally play only a negligible role in the inhibition. Nevertheless, the reactions involving OPCs are very important in these flames.

The sensitivity analysis of the speed of the TMP-doped $H_2/O_2/N_2$ flame to the rate constants of the basic hydrogen combustion reactions and the reaction involving phosphorus compounds revealed the main

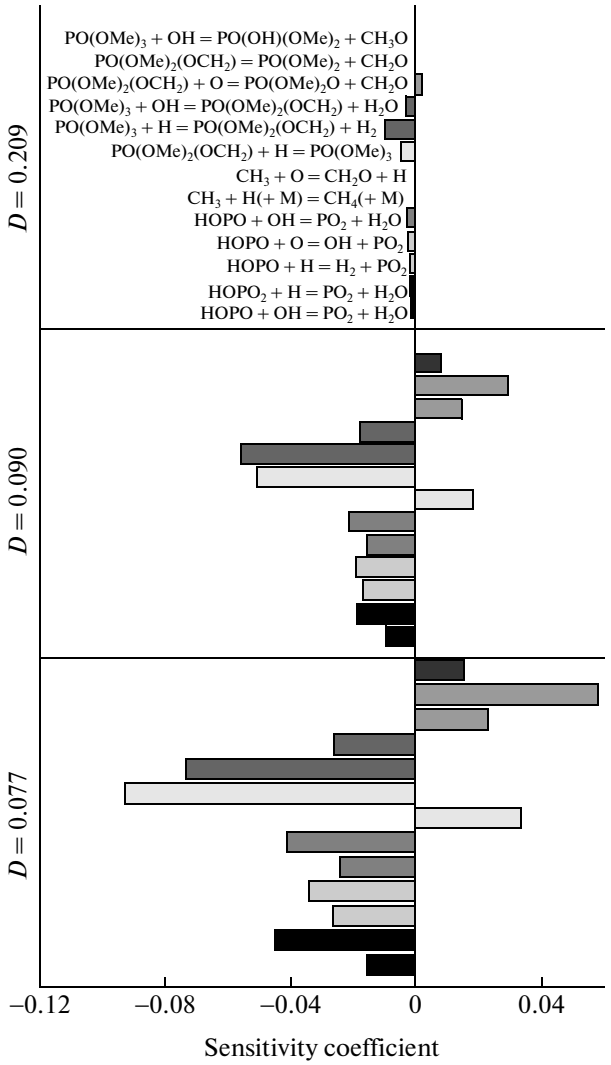

Fig. 5. Sensitivity of the speed of $H_2/O_2/N_2$ flames ($\phi = 1.6$; $D = 0.077$, 0.090, 0.209) doped with 0.04% TMP to the rate constants of the 13 most important reactions of the inhibition mechanism involving phosphorus-containing species.

steps responsible for the increase in F caused by decreasing D. It s clear from the data obtained for the key reactions of hydrogen combustion (Fig. 4) that the main effect of decreasing D is an increasing role of the chain branching reaction $H + O_2 = O + OH^{\bullet}$. At $\phi = 1.6$, the sensitivity coefficient of the flame speed with respect to the rate constant of this reaction increases by a factor of 4 as D decreases from 0.209 to 0.077. In addition, the sensitivity coefficient for this reaction is more than one order of magnitude larger than the sensitivity coefficient for any other reaction. Dilution of the combustible mixture with N_2 changes the role of the recombination reaction $H + O_2(+M) = OH_2^{\bullet}(+M)$, for which the sensitivity coefficient is negative at $D = 0.077$ and 0.090 and positive at $D = 0.209$.

The sensitivity of the flame speed to the rate constants of chain termination reactions—recombination of radicals via their interaction with TMP and its decomposition products (Fig. 5)—increases with decreasing D. For example, the sensitivity coefficients for the constants of reactions (I) and (II) increases by a factor of 8 and 20, respectively, as D decreases from 0.209 to 0.077. This increase is much greater than the increase in sensitivity to the branching rate. According to simulation data, the ratio of the maximum rate of H recombination via reactions (I) and (II) to the maximum rate of the branching reaction increases by a factor of 2.5 as D decreases from 0.209 to 0.077. This is why the inhibition efficiency F increases with decreasing D and, probably, why F increases with increasing ϕ. Thus, the ratio of the chain termination to the chain branching rate is a significant parameter determining the burning velocity of the hydrogen/oxygen flame.

Structure of TMP-Doped Rich $H_2/O_2/N_2$ Flames

The temperature profile and the concentration profiles of stable components (O_2, H_2O), radicals (H, $OH^{\bullet}$), and phosphorus-containing species (PO, HOPO, PO_2, $HOPO_2$) were measured and calculated for a rich $H_2/O_2/N_2$ flame doped with 0.04% TMP at $\phi = 1.6$ and $D = 0.090$. Simulation was carried out using the mechanism presented in [10] with modified rate constants of the above-mentioned reactions (table). The observed and calculated concentration profiles of stable species (O_2, H_2O, TMP), shown in Fig. 6, are in satisfactory agreement (within the confidence interval of the measurements). Figure 7 plots the observed and calculated H and $OH^{\bullet}$ concentration profiles. Varying the rate constants of the reactions listed in the table caused no significant changes in the calculated H and $OH^{\bullet}$ concentration profiles.

The main phosphorus-containing species in the flame 2–15 mm away from the burner are PO and HOPO. Figure 8 presents their concentration profiles in the flame. The PO concentration in the combustion zone increases, passes through a maximum at a distance of 2 mm from the burner, and then falls off down to a nearly zero level at a distance of 6–8 mm. Unlike PO, HOPO accumulates in the flame and is the most abundant phosphorus-containing species. The HOPO concentration increases nonmonotonically, passing through a maximum at a distance of 1.2–1.3 mm from the burner. This shape of the concentration profile is due to the specific features of the model reported in [10]. Calculation of the HOPO formation rate (w) as a function of the height over the burner (Fig. 9) demonstrated that more than 90% of the total amount of

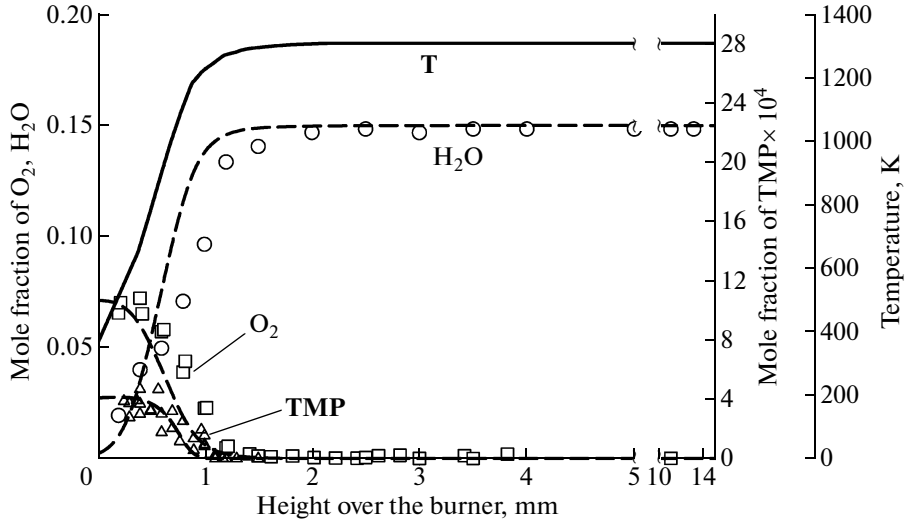

Fig. 6. Temperature and O_2, H_2O, and TMP concentration profiles for the $H_2/O_2/N_2$ flame ($\phi = 1.6$, $D = 0.090$) doped with 0.04% TMP. The points represent experimental data, and the lines represent the results of simulation using the modified mechanism.

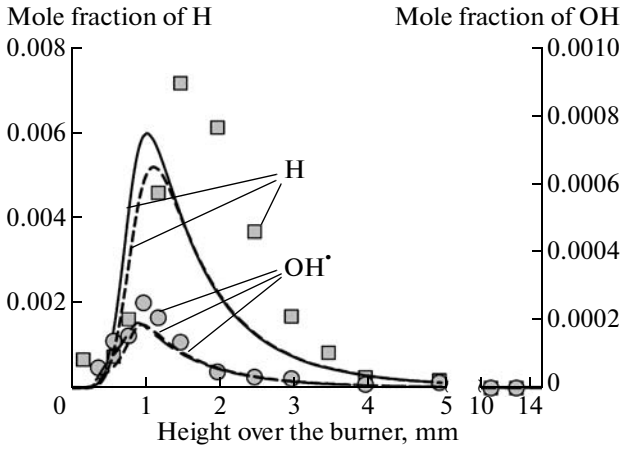

Fig. 7. H and $OH^{\bullet}$ concentration profiles for the $H_2/O_2/N_2$ flame ($\phi = 1.6$, $D = 0.090$) doped with 0.04% TMP. The points represent experimental data, the solid lines represent the results of simulation using the mechanism suggested in [10], and the dashed lines represent the results of simulation using the modified mechanism.

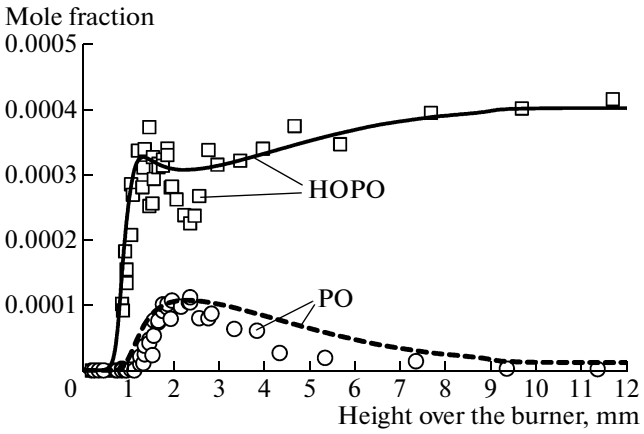

Fig. 8. PO and HOPO concentration profiles for the $H_2/O_2/N_2$ flame ($\phi = 1.6$, $D = 0.090$) doped with 0.04% TMP. The points represent experimental data, and the lines represent the results of simulation using the modified mechanism.

HOPO in the flame results from the reaction $H + PO_2 + M = HOPO + M$. The peak of the HOPO formation rate due to this reaction is at a distance of 1 mm from the burner. HOPO is consumed via a number of reactions. The profiles of the rates of HOPO formation via the several most significant reactions are somewhat farther from the burner. This is due, in part, to the higher activation energies of these reactions. According to [10], the $H + PO_2 + M = HOPO + M$ reaction is characterized by an activation energy of 645 cal/mol and a temperature exponent factor of –2.0, while the activation energy of the main HOPO consumption reactions—$HOPO + H = H_2 + PO_2$ and $HOPO + H = H_2O + PO^{\bullet}$—is 11000 and 8300 cal/mol, respectively.

As a consequence, the profile of the rate of HOPO formation via all reactions (w_Σ) has a maximum at a distance of ~1 mm from the burner and a shallow minimum at 1.6 mm. The latter is responsible for the

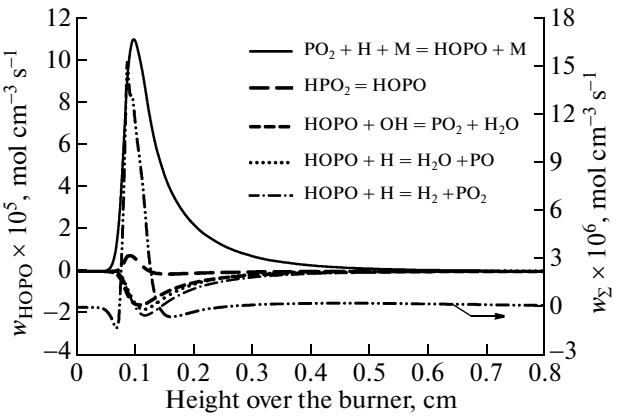

Fig. 9. Rates of HOPO formation and consumption via particular reactions (w) and the total HOPO formation rate (w_Σ) as a function of the height over the burner for the $H_2/O_2/N_2$ flame (ϕ = 1.6, D = 0.090) doped with 0.04% TMP.

HOPO concentration minimum at a distance of 2.2 mm from the burner (Fig. 8).

The simulated flame structure demonstrates that the improved mechanism predicts satisfactorily the measured flame structure.

CONCLUSIONS

This study revealed some specific features of the inhibition mechanism for diluted $H_2/O_2/N_2$ flames at atmospheric pressure. In these flames, as distinct from hydrocarbon flames, the inhibition efficiency in terms of the relative decrease in the flame speed and the relative decrease in the H and $OH^\bullet$ concentrations upon the introduction of the inhibitor into the flame increases with increasing ϕ and with a decreasing dilution ratio D. As follows from our sensitivity analysis, this is due to the increase of the ratio of the rate of chain termination via catalytic processes involving the inhibitor to the chain branching rate. In turn, this is due to the decrease in the flame temperature caused by increasing ϕ and D, which exerts a substantial effect on the chain branching rate and a slighter effect on the catalytic recombination reactions. This temperature effect is explained by the comparatively low activation energies of the reactions responsible for inhibition and the comparatively high activation energy of the branching reaction. The variation in the composition of the phosphorus-containing products in the flame with ϕ also contributes to the inhibition efficiency [10].

The mechanism of flame inhibition by TMP [10] predicts the burning velocity of OPC-doped $H_2/O_2/N_2$ flames with an unsatisfactory accuracy. The sensitivity analysis demonstrated that, in these flames, a significant role is played by reactions of radicals with TMP and with some organophosphorus products. The modification of the rate constants of the most important reactions within the accuracy of their determination enabled us to reconcile the calculated and experimental burning velocity data for the TMP-doped $H_2/O_2/N_2$ flames.

Thus, it was demonstrated for the first time that the mechanism for flame inhibition by OPCs involves both reactions of phosphorus oxides and phosphoric acids ($PO_2 \underset{-H}{\overset{+H}{\rightleftarrows}} HOPO$ and $PO_2 \underset{-OH}{\overset{+OH}{\rightleftarrows}} HOPO_2$ in methane and propane flames) and reactions of OPCs ($(CH_3O)_3PO \underset{+H}{\overset{-H}{\rightleftarrows}} (CH_2O)(CH_3O)_2PO$ in hydrogen/oxygen flames at atmospheric pressure).

REFERENCES

1. Hastie, J.W. and Bonnell, D.W., *Molecular Chemistry of Inhibited Combustion Systems*, National Bureau of Standards Report no. NBSIR 80-2169, 1980, p. 390.
2. Twarowski, A.J., *Combust. Flame*, 1993, vol. 94, p. 91.
3. Werner, J.H. and Cool, T.A., *Combust. Flame*, 1999, vol. 117, p. 78.
4. Glaude, P.A., Melius, C., Pitz, W.J., and Westbrook, C.K., *Proc. Combust. Inst.*, 2002, vol. 29, p. 2469.
5. Wainner, R.T., McNesby, K.L., Daniel, A.W., Miziolek, A.W., and Babushok, V.I., *Halon Options Technical Working Conf.*, Albuquerque, N.M., 2000, p. 141.
6. Shmakov, A.G., Korobeinichev, O.P., Shvartsberg, V.M., Knyazkov, D.A., Bolshova, T.A., and Rybitskaya, I.V., *Proc. Combust. Inst.*, 2005, vol. 30, p. 2345.
7. Mather, J.D., Tapscott, R.E., Shreeve, J.M., and Singh, R.P., *NIST SP 948-3, CD-ROM,* Gann, R.G., Burgess, S.R., Whisner, K.C., and Reneke, P.A., Eds., Gaithersburg, Md.: National Institute of Standards and Technology, 2005.
8. Korobeinichev, O.P., Bolshova, T.A., Shvartsberg, V.M., and Chernov, A.A., *Combust. Flame*, 2001, vol. 125, p. 744.
9. Korobeinichev, O.P., Shvartsberg, V.M., Shmakov, A.G., Bolshova, T.A., Jayaweera, T.M., Melius, C.F., Pitz, W.J., and Westbrook, C.K., *Proc. Combust. Inst.*, 2005, vol. 30, p. 2353.
10. Jayaweera, T.M., Melius, C.F., Pitz, W.J., Westbrook, C.K., Korobeinichev, O.P., Shvartsberg, V.M., Shmakov, A.G., and Curran, H., *Combust. Flame*, 2005, vol. 140, p. 103.
11. Shmakov, A.G., Korobeinichev, O.P., Shvartsberg, V.M., Yakimov, S.A., Knyazkov, D.A., Komarov, V.F., and Sakovich, G.V., *Combust., Explos., Shock Waves*, 2006, vol. 42, no. 6, p. 678.
12. Knyazkov, D.A., Shmakov, A.G., and Korobeinichev, O.P., *Combust. Flame*, 2007, vol. 151, p. 37.
13. Korobeinichev, O.P., Shvartsberg, V.M., Shmakov, A.G., Knyazkov, D.A., and Rybitskaya, I.V., *Proc. Combust. Inst.*, 2007, vol. 31, p. 2741.
14. De Goey, L.P.H., Van Maaren, A., and Quax, R.M., *Combust. Sci. Technol.*, 1993, vol. 92, p. 201.

15. Van Maaren, A., Thung, D.S., and de Goey, L.P.H., *Combust. Sci. Technol.*, 1994, vol. 96, p. 327.
16. Dyakov, I.V., Konnov, A.A., de Ruyck, J., Bosschaart, K.J., Brock, E.C.M., and de Goey, L.P.H., *Combust. Sci. Technol.*, 2001, vol. 172, p. 81.
17. Korobeinichev, O.P., Shvartsberg, V.M., and Chernov, A.A., *Combust. Flame*, 1999, vol. 118, no. 4, p. 727.
18. Korobeinichev, O.P., Tereshchenko, A.G., Shvartsberg, V.M., Chernov, A.A., Zabolotnyi, A.E., and Emel'yanov, I.D., *Combust., Explos., Shock Waves*, 1990, vol. 26, no. 2, p. 173.
19. Korobeinichev, O.P., Ilyin, S.B., Mokrushin, V.V., and Shmakov, A.G., *Combust. Sci. Technol.*, 1996, vol. 116, no. 1, p. 51.
20. Egolfopoulos, F.N. and Law, C.K., *Proc. Combust. Inst.*, 1990, vol. 23, p. 333.
21. Glaude, P.A., Curran, H.J., Pitz, W.J., and Westbrook, C.K., *Proc. Combust. Inst.*, 2000, vol. 28, p. 1749.
22. Rybitskaya, I.V., Shmakov, A.G., and Korobeinichev, O.P., *Combust., Explos., Shock Waves*, 2007, vol. 43, no. 3, p. 253.